The kink effect of the nuclear charge radius in the Relativistic Mean-Field Approximation

Saturnino Marcos[1,*], *Ramón* Niembro[1], and *Mercedes* López-Quelle[2]

[1]University of Cantabria, Department of Modern Physics, 39005 Santander, Spain
[2]University of Cantabria, Department of Applied Physics, 39005 Santander, Spain

Abstract. The kink effect in the nuclear charge radii of lead isotopes is studied using the relativistic mean field approximation with the parameter sets NL3* and NL-Z. It is shown that the small component of the valence neutrons' Dirac spinors plays an essential role in the formation of the kink, due to its effects on the single-proton central potential in both cases. However, notable differences emerge between the results obtained from these two sets when pairing correlations are not considered.

1 Introduction

Some isotopic chains exhibit a sudden change in the increasing nuclear charge radii trend when the neutron number exceeds a specific value [1]. This sudden change is usually referred as a kink or kink effect. The most typical example is found in the charge radii of Pb isotopes. It appears when the neutron number (N) exceeds $N = 126$ [2] (other examples can be seen in [3]). This kink, quite generally, is fairly well reproduced by the relativistic mean-field approximation (RMFA) [2, 4], although not all models reproduce the appropriate magnitude [3]. In contrast, non-relativistic Skyrme-Hartree-Fock (SHF) models with standard parametrisations fail to reproduce it [5].

In Ref. [6], the failure of the standard Skyrme interactions to fit the kink in lead isotopes is related to the somewhat large spin-orbit interaction caused by the isospin dependence of the Skyrme functionals. The spin-orbit interaction affects the relative positions of the neutron $2g_{9/2}$ and $1i_{11/2}$ energy levels, which are the most relevant levels in relation to the kink.

New Skyrme functionals have been proposed by modifying the spin-orbit interaction [6–9]. However, in non-relativistic mean-field functionals, Fayans *et al.* [10, 11] make the surface and pairing terms dependent on density gradients. In recent years, the core swelling [12], the tensor interaction and symmetry energy [9], and the particle-vibration coupling [13] have been considered important mechanisms in relation to the kink. In Refs. [7] and [14], the important role played by the neutron orbit $1i_{11/2}$ (in contrast to $2g_{9/2}$) in the kink of lead isotopes is related to its large overlap with the proton orbits that contribute the most to the kink. However, we have argued that the nucleon-nucleon interaction considered in [7, 14] is not appropriate [15]. A detailed review of the effort made to understand the behaviour of the charge radii in different isotopic families is given in Ref. [4].

In Refs. [15, 16], it is shown within the RMFA that the small component of the valence neutrons' Dirac spinors plays an essential role on the kink formation through its effects on the single-proton central potential. This work aims to continue the study of the relativistic effects in the behaviour of the charge radii of isotopes of lead initiated in [15, 16], using the RMFA with the parameter sets NL3* [17] and NL-Z [18].

2 The relativistic model

In the RMFA, the Dirac spinor $\psi_a(\vec{r})$ for a nucleon with the mass M in the state a satisfies the Dirac equation

$$\{-i\hbar\vec{\alpha}\cdot\vec{\nabla} + \beta[M + S(\vec{r})] + V(\vec{r})\}\psi_a(\vec{r}) = E_a\psi_a(\vec{r}), \quad (1)$$

where $E_a = M + \varepsilon_a$ and $-\varepsilon_a$ represents the binding energy of $\psi_a(\vec{r})$. $S(\vec{r})$ and $V(\vec{r})$ are the scalar and vector single-particle potentials generated by the scalar (σ) and vector (ω, ρ and γ) bosons, respectively. For nuclei with spherical symmetry, that we will assume in this work, $S(\vec{r})$ and $V(\vec{r})$ become central potentials. Then, in the standard notation

$$\psi_a(\vec{r}) = \begin{bmatrix}\phi_a(\vec{r})\\ \zeta_a(\vec{r})\end{bmatrix} = \frac{1}{r}\begin{bmatrix}iG_a(r)\\ F_a(r)\vec{\sigma}\cdot\hat{\mathbf{r}}\end{bmatrix} y^{m_a}_{j_a l_a}(\hat{\mathbf{r}})\chi^a_{\frac{1}{2}}, \quad (2)$$

where $\frac{G_a(r)}{r}$ and $\frac{F_a(r)}{r}$ represent the radial part of the large and small components, respectively.

We consider the Schrödinger-like equation equivalent to the Dirac equation [16]:

$$\left[-\frac{\hbar^2}{2M}\nabla^2 + V_{\text{cent}}(r,\varepsilon) + V_{\text{SO}}(r,\varepsilon)\right]\tilde{\phi}(\vec{r}) = \varepsilon\tilde{\phi}(\vec{r}), \quad (3)$$

where the subscript a is dropped for simplicity, and $\tilde{\phi}(\vec{r}) = B(r)^{-1/2}\phi(\vec{r})$, with $B(r) \equiv 2M + \varepsilon + S(r) - V(r)$.

*e-mail: marcoss@unican.es

The central potential $V_{\rm cent}(r,\varepsilon)$ can be written as

$$V_{\rm cent}(r,\varepsilon) = S + V + V^{\rm rel}_{\rm cent}(r,\varepsilon) \equiv V_{\rm cent^*}(r) + V^{\rm rel}_{\rm cent}(r,\varepsilon), \quad (4)$$

where $V_{\rm cent^*}(r)$ is state independent and $V^{\rm rel}_{\rm cent}(r,\varepsilon)$ contains small relativistic terms $\propto 1/M$.

The NL3* and NL-Z parameter sets share the same Lagrangian structure. Their main differences lie in the σ-meson mass (m_σ) and the meson-field coupling constants. Thus, $m_\sigma^{\rm NL3^*} = 502.57$ MeV is larger than $m_\sigma^{\rm NL-Z} = 488.67$ MeV. The saturation nuclear matter parameters (in standard notation) are as follows: For the NL3* set: $\rho_0 = 0.150$ fm^{-3}, $E/A = -16.31$ MeV, $K = 258.27$ MeV, and $a_4 = 38.68$ MeV. For the NL-Z set: $\rho_0 = 0.151$ fm^{-3}, $E/A = -16.185$ MeV, $K = 173.5$ MeV, and $a_4 = 41.8$ MeV.

3 Results

The isotopic shift of the charge radius of lead isotopes, relative to ^{208}Pb, is defined as

$$\Delta\langle r_c^2\rangle = r_c^2(^A\text{Pb}) - r_c^2(^{208}\text{Pb}), \quad (5)$$

where $r_c^2(^A\text{Pb})$ represents the mean-square charge radius of the lead isotope ^{A}Pb.

The results of $\Delta\langle r_c^2\rangle$ for the NL3* and NL-Z parameter sets are shown in Fig. 1. For $A > 208$, we have considered the valence neutrons alternatively occupying the $1i_{11/2}$ level (i-conf.) or the $2g_{9/2}$ level (g-conf.), with $F_{1i_{11/2}}$ and $F_{2g_{9/2}}$ either zero or nonzero.

For $F_a \neq 0$, the NL-Z set yields a larger kink than the NL3* set for the i-conf., probably due to its larger value of a_4 and lower compressibility modulus [19, 20]. However, when pairing correlations are considered, the differences in the kink almost disappear. This occurs because they are compensated by the effects of the different occupancies of the $1i_{11/2}$ and $2g_{9/2}$ levels, due to their different binding energies in both sets, as shown in Fig. 2. Thus, the two sets provide a good description of the kink in lead isotopes, even though the energies of the $1i_{11/2}$ and $2g_{9/2}$ levels differ by about 250 keV and are practically *interchanged*. This result refines the claim in [21] that "the reproduction of the empirical kink in isotope shifts of even Pb nuclei by relativistic effective interactions points to the occurrence of pseudospin symmetry in single-neutron spectra in nuclei" (which implies the quasi-degeneracy of these two levels), as it shows that two models, in which $E_{1i_{11/2}} - E_{2g_{9/2}}$ differs by 532 keV, can achieve kinks with similar magnitudes.

Fig. 1 also reveals that the contributions of the small components $F_{1i_{11/2}}$ and $F_{2g_{9/2}}$ to the kink are essential for reproducing the experimental magnitude of the kink. For the g-conf., this contribution is considerably larger for the NL-Z set than for NL3* (see discussion below).

To quantify the magnitude of the kink in lead, we introduce the kink indicator defined as

$$\xi = \frac{r_c^2(^{210}\text{Pb}) - r_c^2(^{208}\text{Pb})}{r_c^2(^{208}\text{Pb}) - r_c^2(^{206}\text{Pb})}. \quad (6)$$

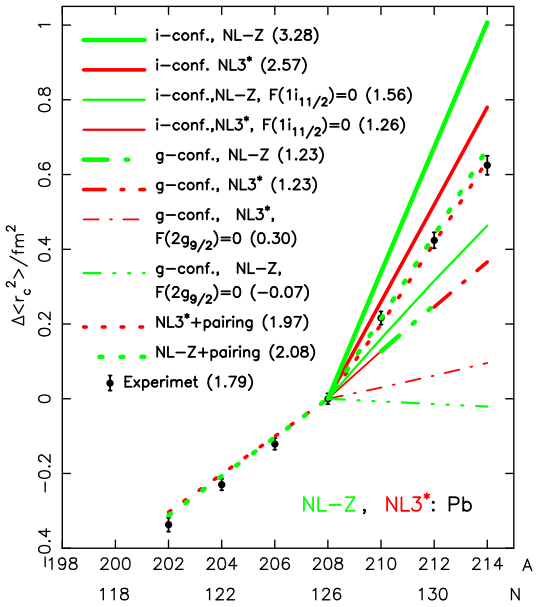

Figure 1. The isotope shift $\Delta\langle r_c^2\rangle$ for lead (A even), calculated within the RMFA using the parameter sets NL3* and NL-Z, is plotted for the "i-conf." and "g-conf." configurations. If indicated, calculations assume $F_{1i_{11/2}} = 0$ and $F_{2g_{9/2}} = 0$. Pairing correlations for neutrons within the BCS approximation [22] are also considered, assuming constant pairing matrix elements and experimental gap values. For $N < 126$, all neutron levels between the shell gaps at $N = 50$ and $N = 126$ are included in this calculation. For $N > 126$, The seven bound neutron levels above the shell gap at $N = 126$ are taken into account. The experimental values are taken from Ref. [1]. Extrapolated values for non-integer A are shown to guide the eye. For each case considered, the kink indicator, ξ, from (Eq. 6) is given in parentheses.

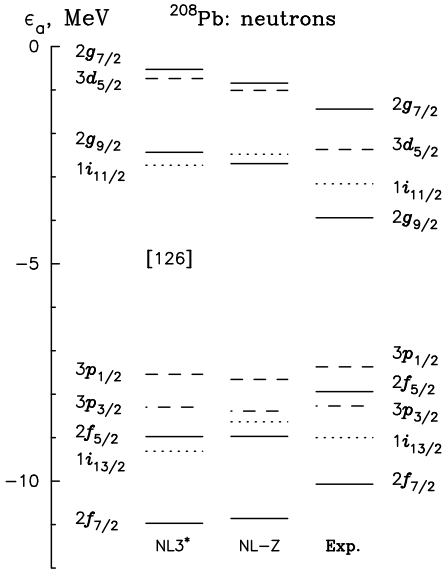

Figure 2. Single-neutron energies of the ^{208}Pb nucleus calculated in the RMFA with the NL3* and NL-Z parameter sets. The experimental values shown in the column labelled Exp. are taken from Ref. [23].

The values for the different cases considered in Fig. 1 are given in parentheses. The results, including pairing ef-

fects, can be compared with those for lead presented in Fig. 6 of [3] and in Table VI of [9][1]. These sources show predictions from several relativistic models and from the non-relativistic TFFS-Fayans functional [3]. Three of the four relativistic models (PC-L3R, PC-X, DD-PCX, and DD-MEX) overestimate the kink indicator ξ, while the fourth predicts a Z dependence of ξ that is not observed experimentally. In [9], ten relativistic models in the Hartree and Hartree-Fock approximations are considered. Most of them, predict the energy of the $1i_{11/2}$ level below that of the $2g_{9/2}$. The predictions for the energy of these levels of the NL3* and NL-Z functionals are intermediate between those considered in [9]. Both the energies of the $1i_{11/2}$ and $2g_{9/2}$ levels and their occupation probabilities (for A>208) resemble those of the DD-ME2 models. The occupation probabilities of these levels for the NL3* and NL-Z functionals are, respectively, 0.090 and 0.056 for the former and 0.083 and 0.065 for the latter.

Fig. 3 shows $G(r)$ and $F(r)$ for the $1i_{11/2}$ and $2g_{9/2}$ orbitals of ^{208}Pb for the NL3* and NL-Z sets. For $N > 126$, the contribution from the neutrons in these orbitals to the baryonic and scalar densities determines their contribution to the central potential of protons.

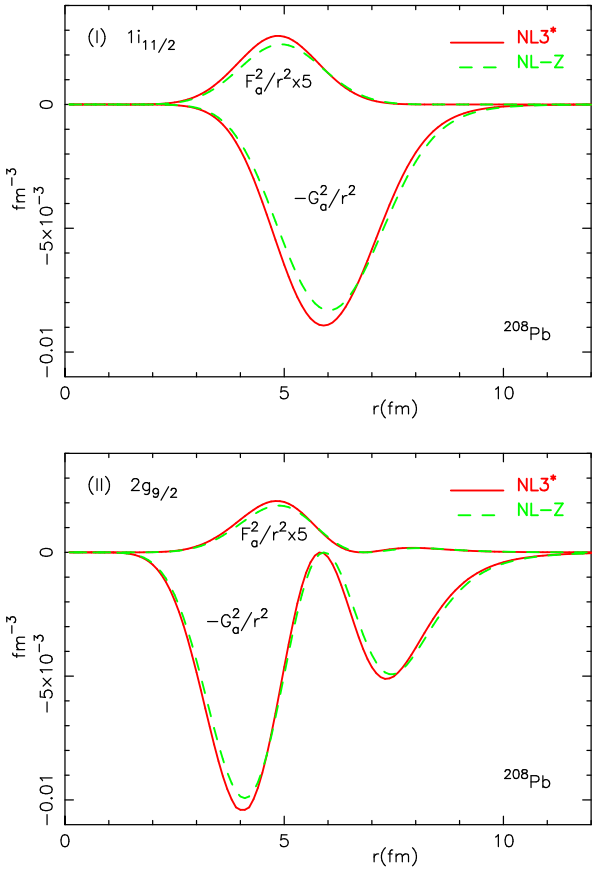

Figure 3. Quantities $-G_a^2/r^2$ and F_a^2/r^2 corresponding to the empty orbitals $1i_{11/2}$ (panel I) and $2g_{9/2}$ (panel II) in the ^{208}Pb nucleus for the NL3* and NL-Z parameter sets.

[1]Notice that $\Delta R^Z_{ch}(A)$, as defined in [9], can be expressed for lead as $\Delta R^Z_{ch}(A) = |\Delta\langle r_c^2(A)\rangle|/2R^Z_{ch}(208)$.

Fig. 4 shows the (non-self-consistent) contributions of a hypothetical neutron in the empty orbitals $a = 1i_{11/2}$ and $a = 2g_{9/2}$ of the ^{208}Pb nucleus to $V_{\text{cent}^*}(r)$ for protons, from the large (G_a), small (F_a), and combined ($G_a + F_a$) components, using the NL3* and NL-Z sets. It can be seen that the contributions to the potential of the large and small components are nearly proportional to the quantities $-G_a^2/r^2$ and F_a^2/r^2, respectively, but with a proportionality factor about five times larger for the small component than for the large one. This is because the contributions of the scalar and vector fields to the central potential are large and have opposite signs. This fact is the main reason for achieving saturation in nuclear matter and the large magnitude of the kink in lead isotopes in the RMFA [16].

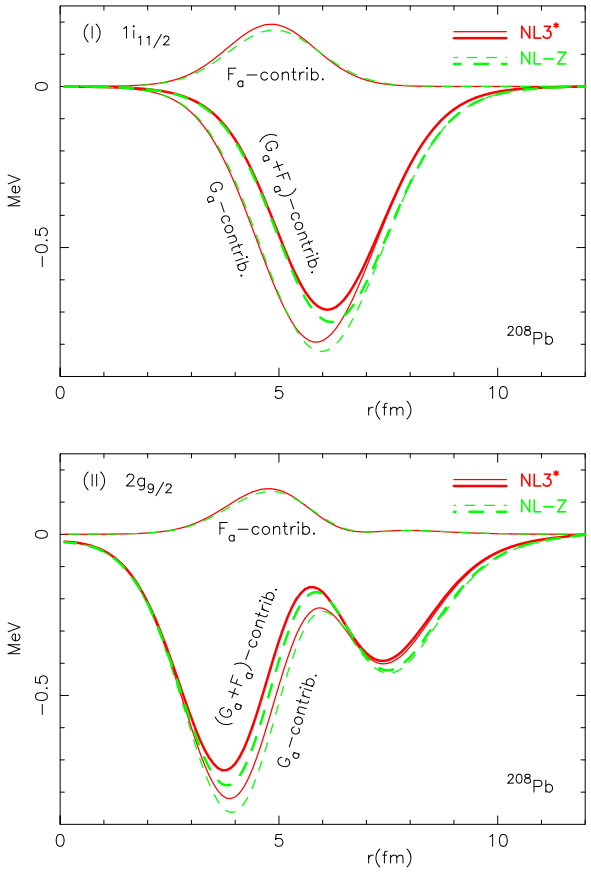

Figure 4. Panel (I): Contributions (non-self-consistent) of a hypothetical neutron in the empty orbital $a = 1i_{11/2}$ of the ^{208}Pb nucleus to $V_{\text{cent}^*}(r)$ for protons, from the large (G_a, thinner lines with negative values); small (F_a, thinner lines with positive values); and combined ($G_a + F_a$, thicker lines) components with the NL3* and NL-Z sets. Panel (II): Same as Panel (I) but for the empty orbital $a = 2g_{9/2}$.

Fig. 5(I) shows the variation of the proton central potential $V_{\text{cent}^*}(r)$, $\delta V_{\text{cent}^*}(r)$, when six neutrons are added to the ^{208}Pb nucleus to form ^{214}Pb in the i-conf., considering $F_{1i_{11/2}} = 0$, for the NL3* and NL-Z sets. It includes the self-consistent effects. Note that $V_{\text{cent}^*}(r)$ and, consequently, $\delta V_{\text{cent}^*}(r)$ are independent of the proton orbital (see Eq. (4)). The form of $\delta V_{\text{cent}^*}(r)$ suggests that these six

neutrons will increase the nuclear charge radius, as confirmed in Fig. 1.

Fig. 5(II) shows the same quantity as Fig. 5(I), but with the contribution of the small component $F_{1i_{11/2}}$ also taken into account. It considerably increases $\delta V_{\text{cent}^*}(r)$ around the maximum of $F^2_{1i_{11/2}}/r^2$ (see Figs. 3(I) and 4(I)) and shifts the minimum of $\delta V_{\text{cent}^*}(r)$ to larger values of r. These two effects lead to a notable increase in the nuclear charge radius as neutrons are added to the $1i_{11/2}$ orbital of Pb nuclei, which is crucial for reproducing the observed magnitude of the kink in lead isotopes. The relevance of the self-consistent effects of the valence neutrons in this orbital for their contribution to $\delta V_{\text{cent}^*}(r)$ becomes even more evident when the contribution of $F^2_{1i_{11/2}}/r^2$ is included than when it is not.

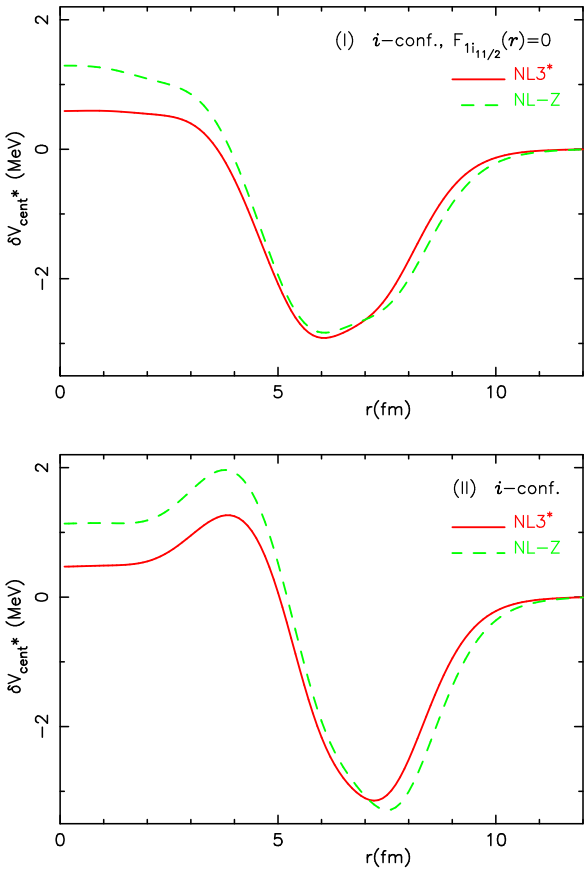

Figure 5. The quantity $\delta V_{\text{cent}^*}(r)$ for protons when six neutrons are added to the ^{208}Pb nucleus to form ^{214}Pb in the i-conf. for the NL3* and NL-Z sets. In Panel (I), $F_{1i_{11/2}} = 0$ is considered, while in Panel (II), $F_{1i_{11/2}} \neq 0$. Note that $\delta V_{\text{cent}^*}(r)$ is independent of the proton orbital.

Fig. 6(I) shows the same quantity as Fig. 5(I), but considering the six valence neutrons in the $2g_{9/2}$ orbital of ^{214}Pb instead of in the $1i_{11/2}$ orbital, with $F_{2g_{9/2}} = 0$. It can be expected that the two minima of $\delta V_{\text{cent}^*}(r)$ are expected to attract protons, leading to competition between them. As the inner minimum of $\delta V_{\text{cent}^*}(r)$ for the NL-Z set is deeper than that of the NL3* set, $\Delta\langle r_c^2(^{214}\text{Pb})\rangle$ will be smaller for the NL-Z set compared to NL3* set. This is shown in Fig. 1.

Fig. 6(II) shows the same quantity as Fig. 6(I), but it also accounts for the effect of the small component $F_{2g_{9/2}}$, which reduces the depth of the inner minimum of $\delta V_{\text{cent}^*}(r)$ (more for the NL-Z set than for NL3*) and increases the depth of the outer minimum (see Figs. 3(II) and 4(II)). As a result, the nuclear charge radius of ^{214}Pb increases considerably due to the six valence neutrons in the $2g_{9/2}$ orbital, with a greater increase for the NL-Z set than for NL3*. The relevance of the self-consistent effects of the valence neutrons in the $2g_{9/2}$ orbital for their contribution to $\delta V_{\text{cent}^*}(r)$ also becomes more evident when the contribution of $F^2_{2g_{9/2}}/r^2$ is included than when it is not.

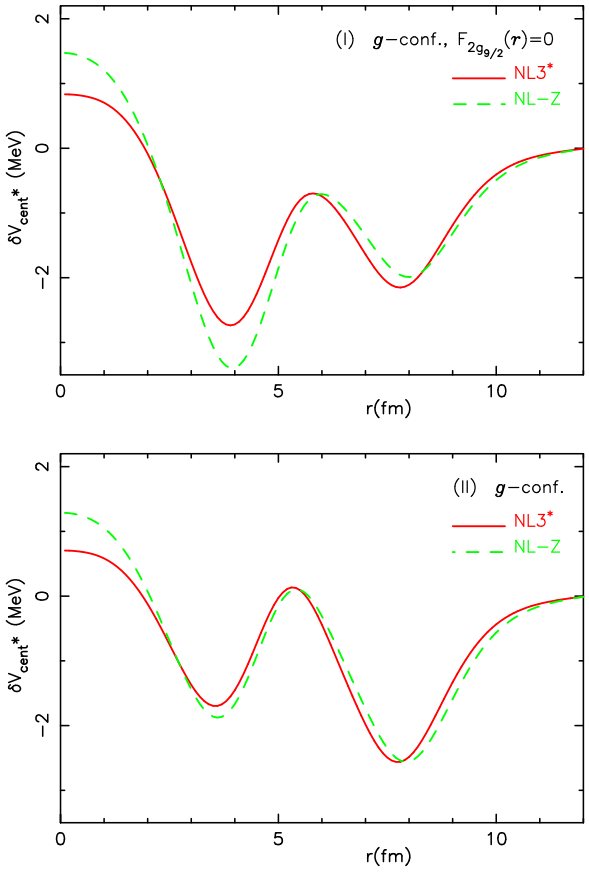

Figure 6. The same as Fig. 5, but for the g-conf., i.e., for the six valence neutrons in the $2g_{9/2}$ orbital.

Fig. 1 shows that the small component contribution of the valence neutrons in the $1i_{11/2}$ orbital (i-conf.) to the kink indicator ξ is approximately 1.72 and 1.31 for the NL-Z and NL3* functionals, respectively. In contrast, when the neutrons occupy the $2g_{9/2}$ orbital (g-conf.), this contribution is about 1.3 and 0.93, respectively. Thus, in all cases considered, the small component contribution to ξ is highly significant compared to the corresponding theoretical results, which include pairing effects, as well as the experimental value.

To understand the results presented in Figs. 1, 4, 5, and 6, it is important to note that in relativistic models, the contributions of the small ($F(r)$) and large ($G(r)$) components of a given Dirac spinor corresponding to a valence neutron

state to the nucleon density are proportional to $F^2(r)/r^2$ and $G^2(r)/r^2$, respectively. In contrast, for the NL3* and NL-Z functionals employed in this study, their contributions to the proton central potential are approximately proportional to $5 \times F^2(r)/r^2$ and $G^2(r)/r^2$, respectively [16]. Therefore, although the contribution of $F(r)$ to the nucleon density is relatively minor, its effect on the central potential is non-negligible in all relativistic models.

From the results presented above, it can be inferred that the small component of the valence-neutron Dirac spinors does not directly influence the odd-even staggering (OES) of nuclear charge radii. This is because, in our calculations, this component remains similar for a paired or unpaired neutron in a given orbital, regardless of whether the isotope has an even or odd N, respectively. A detailed study of this effect requires going beyond the RMFA used in this work [24, 25]. However, if it is assumed that the particle-vibration coupling (PVC) effect in lead isotopes with $N(\text{odd}) > 126$ reduces the energy of the unpaired neutron in the $2g_{9/2}$ orbital more than in the $1i_{11/2}$ orbital [25], then this would favour the occupancy of the former over the latter. Consequently, the nuclear charge radius will increase with N relatively less for isotopes with odd N than for their neighbors with even N, leading to the emergence of OES. The relative energy ordering of these orbitals in Fig. 2 favours this effect for the NL3* set compared to the NL-Z set. However, since the kink effect for the i-conf. is stronger in the NL-Z set than in the NL3* set, a certain degree of compensation can be expected.

4 Conclusions

In the RMFA, considering the parameter sets NL3* and NL-Z, we have investigated the relativistic effects on the kink of the nuclear charge radius of lead. In both cases, the contribution of the small component of the valence neutron orbitals for $A > 208$ is essential for reproducing the kink observed in experiments. The results reveal why the i-conf. produces a more pronounced kink than the g-conf. This is because, in the latter case, two minima appear in the variation of the central potential as neutrons are added to the $2g_{9/2}$ orbital, which compete to attract protons.

Significant differences in the kink appear between the NL3* and NL-Z parameter sets for the i-conf. and g-conf., which partially compensate for each other, leading to a good description of the kink in both cases when pairing correlations are included. The effect of the small component of the $2g_{9/2}$ neutron orbital on the kink is significantly larger for the NL-Z set than for NL3*. The effects of the valence neutrons on the kink across $V^{\text{rel}}_{\text{cent}}(r, \varepsilon)$ are observable but much smaller than those across $V_{\text{cent}^*}(r)$.

References

[1] I. Angeli, At. Data Nucl. Data Tables **99**, 69 (2013).
[2] M. M. Sharma, G. A. Lalazissis, P. Ring, Phys. Lett. B **317**, 9 (1993).
[3] Z. Yue *et al.*, Phys. Rev. C **110**, 034315 (2024).
[4] U. C. Perera, A. V. Afanasjev, P. Ring, Phys. Rev. C **104**, 064313 (2021).
[5] N. Tajima, P. Bonche, H. Flocard, P.-H. Heenen, and M. Weiss, Nucl. Phys. A **551**, 434 (1993).
[6] P.-G. Reinhard, H. Flocard, Nucl. Phys. A **584**, 467 (1995).
[7] M. Goddard, P. D. Stevenson, A. Rios, Phys. Rev. Lett. **110**, 032503 (2013).
[8] H. Nakada, T. Inakura, Phys. Rev. C **91**, 021302(R) (2015).
[9] T. Naito, T. Oishi, H. Sagawa, Z. Wang, Phys. Rev. C **107**, 054307 (2023).
[10] S. A. Fayans, S. V. Tolokonnikov, E. L. Trykov, D. Zawischa, Nucl. Phys. A **676**, 49 (2000).
[11] P.-G. Reinhard, W. Nazarewicz, Phys. Rev. C **95**, 064328 (2017).
[12] W. Horiuchi, T. Inakura, Phys. Rev. C **105**, 044303 (2022).
[13] T. Day Goodacre *et al.*, Phys. Rev. C **104**, 054322 (2021).
[14] U. C. Perera, A. V. Afanasjev, Phys. Rev. C **107**, 064321 (2023).
[15] S. Marcos, R. Niembro, M. López-Quelle, Nucl. Phys. A **1047**, 122883 (2024).
[16] S. Marcos, R. Niembro, M. López-Quelle, Eur. Phys. J. A **60**, 78 (2024).
[17] G. A. Lalazissis, S. Karatzikos, R. Fossion, D. Pena Arteaga, A. V. Afanasjev, P. Ring, Phys. Lett. B **671**, 36 (2009).
[18] M. Rufa, P.-G. Reinhard, J. A. Maruhn, W. Greiner, M. R. Strayer, Phys. Rev. C **38**, 390 (1988).
[19] R. Niembro, S. Marcos, M. López-Quelle, L. N. Savushkin, Phys. At. Nucl. **75**, 269 (2012).
[20] S. Marcos, L. N. Savushkin, M. López-Quelle, R. Niembro, and P. Bernardos, Phys. Lett. B **507**, 135 (2001).
[21] J.-P. Ebran, A. Mutschler, E. Khan, and D. Vretenar, Phys. Rev. C **94**, 024304 (2016).
[22] P. Ring, P. Schuck, *The Nuclear Many-Body Problem* (Springer, Berlin, 1980).
[23] V. I. Isakov, Phys. Part. Nucl. **38**, 269 (2007).
[24] E. V. Litvinova, A. V. Afanasiev, Phys. Rev. C **84**, 014305 (2011).
[25] T. Day Goodacre *et al.*, Phys. Rev. Lett. **126**, 032502 (2021).